Theory of Nonlinear Photoconductive Sampling in Atomic Gases

Manoram Agarwal, Armin Scrinzi, Ferenc Krausz, and Vladislav S. Yakovlev*

The formation and evolution of electron wave packets in the process of strong-field ionization is one of the major research topics in attosecond science. The recently developed technique of nonlinear photoconductive sampling (NPS) requires a detailed understanding of these dynamics and provides a new approach to studying them. This work is motivated by the lack of a solid theoretical foundation for NPS measurements. The analysis shows that, for NPS in atomic gases, the strong-field approximation provides an adequate description of the ionization dynamics but makes a significant error in predicting the spectral response function because the Coulomb interaction between photoelectrons and their parent ions significantly affects the motion of the electron wave packets.

1. Introduction

One of the early achievements of attosecond physics was the direct measurement of light waves,[1] where the photoionization of atoms by a subfemtosecond pulse of extreme ultraviolet light was used to sample the electric field of a few-cycle laser pulse. While powerful, this method has been accessible to only a few laboratories—both attosecond pulse generation and photoionization measurements require an expensive vacuum infrastructure in addition to a laser system capable of producing intense, few-cycle laser pulses with a stabilized carrier-envelope phase (CEP). Recently, several much simpler techniques for sampling broadband optical fields have been invented.[2–10] These techniques still rely on CEP-stabilized laser pulses, but they do not use attosecond bursts of extreme ultraviolet light. Each of these techniques takes advantage of some fast nonlinear phenomenon that confines the nonlinear interaction of a few-cycle intense laser pulse with a much weaker field of a probe pulse to a time interval much shorter than any optical cycle in either pulse. One of these techniques is nonlinear photoconductive sampling (NPS),[7] which takes advantage of a rapid change in the conductivity of a medium[11] caused by strong-field (multiphoton or tunneling) ionization. In this technique, the ionizing and probe fields are linearly polarized and orthogonal to each other (see Figure 1). The central part of the gating pulse generates free-moving charges by ionizing gas atoms or photoinjecting carriers in a wide bandgap solid. The probe pulse accelerates the charges so that they acquire displacement and velocity along the direction of the probe field. As a result, a macroscopic electric dipole is formed, whose field can be measured by placing one or more electrodes close to it and detecting the induced mirror charge.[12] Due to the high nonlinearity of strong-field ionization, the bandwidth of NPS exceeds one petahertz.[7] This large bandwidth is understood to be a consequence of subfemtosecond peaks in the time-dependent ionization rate—most free charges appear at the peaks of the ionizing electric field, and their generation is confined to time intervals significantly shorter than a half-cycle of the field oscillation.

To take full advantage of the PHz bandwidth of NPS, its spectral response function must be known. From a theoretical point of view, there are two fundamental problems. First, it is essential to know the ionization rate, for which many models exist, but it is not clear from the existing literature which one is most appropriate for describing NPS measurements. Second, the Coulomb attraction between a free electron and its parent ion is known to play an important role in strong-field physics, but the effect of this interaction on NPS measurements was not explored.

In this paper, we present a systematic theoretical analysis of an idealized NPS measurement, where the measured signal is assumed to be proportional to the drift electric current formed by the ionization of gas atoms and the acceleration of the electrons by the probe pulse. Within the strong-field approximation (SFA), we derive expressions for the dependence of the drift current on the gate-probe delay. From these equations, we obtain an analytical result for the ionization rate. A comparison of the SFA results with that of the numerical solution of the time-dependent Schrödinger equation (TDSE) allows us to study the role of the Coulomb attraction between a free electron and its parent ion.

M. Agarwal, F. Krausz, V. S. Yakovlev
Attosecond Physics
Max-Planck-Institut für Quantenoptik
Hans-Kopfermann-Str. 1, 85748 Garching, Germany
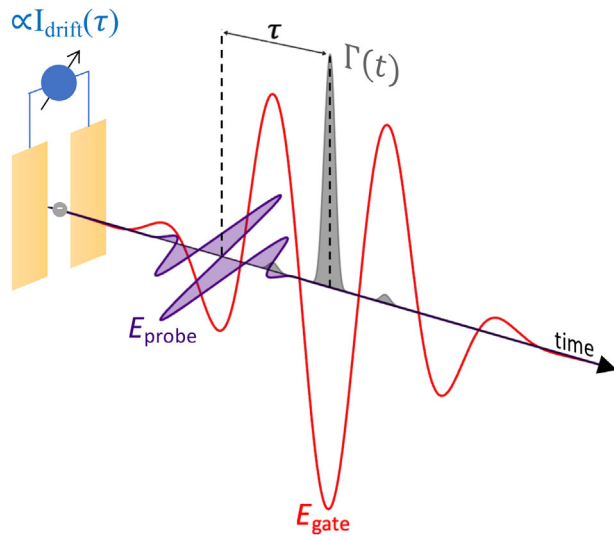E-mail: vladislav.yakovlev@mpq.mpg.de

A. Scrinzi
Faculty of Physics
Ludwig-Maximilians-Universität München
Theresienstrasse 37, 80333 Munich, Germany

F. Krausz, V. S. Yakovlev
Faculty of Physics
Ludwig-Maximilians-Universität München
Am Coulombwall 1, 85748 Garching, Germany

**ADVANCED
SCIENCE NEWS**
_____
www.advancedsciencenews.com

*annalen
der* **physik**
www.ann-phys.org

Figure 1. Schematic of nonlinear photoconductive sampling. An atom is exposed to a strong gate pulse (red) polarized along the z-axis and a weak probe pulse (blue) polarized along the x-axis. The electric field of the gate pulse ionizes atoms via multiphoton absorption or tunneling. The electric field of the probe pulse accelerates the free electrons along the x-axis.

We find that this electron-ion interaction must be taken into account to fully exploit the potential of NPS for measuring broadband waveforms.

2. A General Description of Photoconductive Sampling

There are two pulses involved in photoconductive-sampling measurements: a gate pulse that detaches electrons from atoms within a possibly short time window, and a weak, linearly polarized probe pulse that accelerates photoelectrons but does not ionize atoms on its own. When photoconductive sampling is applied for optical-field detection, the goal is to measure the electric field of the probe pulse by observing a signal resulting from the displacement of photoelectrons caused by their interaction with the probe field. For this scheme to work reliably, it is helpful to minimize the effect of the gate pulse on the electron motion along the direction of the probe field. In the case of nonlinear ionization, which requires strong electric fields, the field of the gate pulse must be orthogonal to the probe field. In the following, we will denote the gate and probe fields as $E_z(t)$ and $E_x(t)$, respectively.

If an electron were a classical particle starting its free motion at a birth time t_b, then by the end of its interaction with the probe field, it would acquire the following drift velocity along the x-axis:

$$v_{\mathrm{drift}}(t_b) = -\frac{e}{m_e} \int_{t_b}^{\infty} E_x(t') \, dt' = -\frac{e}{m_e} A_x(t_b) \tag{1}$$

Here, $e > 0$ is the elementary charge, m_e is the mass of the electron and $A(t)$ is the vector potential defined by $E(t) = -A'(t)$. If we could confine photoionization to a time interval that is much shorter than the fastest oscillation in $E_x(t)$ and measure how the drift velocity depends on the gate-probe delay, then, within this simple model, the measured signal would be proportional to the

vector potential of the probe pulse. The physics that relates the acceleration of charges by the probe field to the measured signal is complicated; it involves the formation of a macroscopic dipole, the field of which interacts with a nearby electrode, causing some charge to flow through a circuit connected to the electrode. Although mean-field charge interactions and electron-atom scattering affect the magnitude of the measured signal and its dependence on the gas pressure[12] they have little effect on the delay dependence of the signal because they unfold on time scales that exceed the duration of the probe pulse by orders of magnitude. For our theoretical analysis, we will assume that the x component of the drift electric current in single-atom simulations is the observable relevant to NPS measurements and focus our attention on improving the oversimplified model embodied in Equation (1).

We first need to account for the fact that photoionization can occur at any time during the gate pulse, although nonlinear ionization is most probable when the electric field of the gate pulse is close to its peak value. This is done by introducing an ionization rate $\Gamma(t)$, which we regard as the probability density of ionization at time t. Although the concept of ionization rate is widely used to describe photoionization, it is controversial because there is no unique way to define the ionization probability in the presence of a strong electric field. We will show later how to solve this problem in the context of photoconductive sampling within the strong-field approximation. For now, we simply assume that a meaningful definition of $\Gamma(t)$ exists and that this quantity does not depend on the probe field. If the Coulomb interaction between a photoelectron and its parent ion were negligible, then the density of the drift electric current along the probe field would be given by

$$I_{\mathrm{drift}}(\tau) = \frac{e^2 N_{\mathrm{at}}}{m_e} \int_{-\infty}^{\infty} \Gamma(t_b - \tau) A_x(t_b) \, dt_b \tag{2}$$

where N_{at} is the concentration of atoms and τ is the gate-probe delay, which we define as the arrival time of the gate pulse. In the frequency domain, we can write Equation (2) in this form

$$I_{\mathrm{drift}}(\omega) = \frac{e^2 N_{\mathrm{at}}}{m_e} A_x(\omega) G^*(\omega) \tag{3}$$

Here we have denoted the Fourier transform of $\Gamma(t)$ by $G(\omega)$ because Equation (3) is more general than the classical model, which we have used mostly for pedagogical reasons. This equation is a general description of a linear relationship between A_x and I_{drift}. Therefore, it must be valid also in quantum mechanics as long as the probe field is so weak that its interaction with electrons can be considered linear. Note that this requirement allows the interaction with the gate field to be very nonlinear and even nonperturbative. From this point of view, $G(\omega)$ is the spectral response function of NPS measurements, while its time-domain counterpart $G(t)$ is a gating function, which may or may not have the meaning of an ionization rate.

The main assumption that we made in deriving Equation (2) was to neglect the Coulomb interaction between the electron and the ion. Let us search for a suitable ansatz that would incorporate this interaction into our formalism. An optical gate field that is strong enough to drive multiphoton ionization quickly removes

**ADVANCED
SCIENCE NEWS**

www.advancedsciencenews.com

annalen
der **physik**

www.ann-phys.org

a photoelectron from the region where the interaction is significant. If the time that it takes an electron to escape the ion's vicinity is much shorter than the period of the probe field, then the value of the field at the birth moment largely determines the effect of the Coulomb interaction on the drift velocity. This consideration suggests the following ansatz

$$
I_{\text{drift}}(\tau) = \frac{e^2 N_{\text{at}}}{m_{\text{e}}} \left(\int_{-\infty}^{\infty} \Gamma(t_{\text{b}} - \tau) A_x(t_{\text{b}}) \, dt_{\text{b}} \right.
$$
$$
\left. - \int_{-\infty}^{\infty} G_{\text{C}}(t_{\text{b}} - \tau) E_x(t_{\text{b}}) \, dt_{\text{b}} \right) \tag{4}
$$

where $G_{\text{C}}(t)$ is the Coulomb gate, which can also describe the effect of the Coulomb interaction on electron-ion recollisions. In the frequency domain, we can keep Equation (3) as it is and define

$$
G(\omega) = \Gamma(\omega) + i\omega G_{\text{C}}(\omega) \tag{5}
$$

where we have used $E_x(\omega) = i\omega A_x(\omega)$.

3. Strong-Field Approximation

In the strong-field approximation, the electron-ion Coulomb interaction is neglected as soon as photoionization occurs, allowing the time-dependent Schrödinger equation to be solved analytically.[13] In the absence of the interaction, Equation (2) serves as an ansatz for interpreting quantum results. This allows us to *define* the ionization rate, $\Gamma(t)$, as a quantity that, once convolved with the vector potential of a probe field yields $I_{\text{drift}}(\tau)$ according to Equation (2). This definition obviates the need to calculate ionization probabilities during the interaction with a strong field. Since the drift velocity of an electron is an unambiguously defined physical observable, our definition of the ionization rate within the SFA is also unambiguous.

In Appendix A, we derive the following equations for the ionization rate

$$
\Gamma_{\text{SFA}}(t) = \Gamma_1(t) + \Gamma_2(t) + \Gamma_3(t) \tag{6}
$$

$$
\Gamma_1(t) = 2 \int_0^{\infty} dp \, p^2 \int_0^{\pi} d\theta \sin\theta \int_{-\infty}^{\infty} dT \, g_0(t, T, p, \theta) \tag{7}
$$

$$
\Gamma_2(t) = -2i \int_0^{\infty} dp \, p^4 \int_0^{\pi} d\theta \sin^3\theta \int_{-\infty}^{\infty} dT \int_{-T}^{T} dt'
$$
$$
\times \left[g_2(t + t', T, p, \theta) - g_2(t, T, p, \theta) \right] \tag{8}
$$

$$
\Gamma_3(t) = 2 \frac{\partial}{\partial t} \int_0^{\infty} dp \, p^3 \int_0^{\pi} d\theta \sin^2\theta \int_{-\infty}^{\infty} dT
$$
$$
\times \left[h(t, T, p, \theta) + h^*(t, -T, p, \theta) \right] \tag{9}
$$

where we have used atomic units and $\boldsymbol{d}(\boldsymbol{p})$ is the dipole matrix element that is responsible for transitions from the ground atomic state to the continuum state with the (asymptotic) momentum $\boldsymbol{p} = (\boldsymbol{e}_z \cos\theta + \boldsymbol{e}_x \sin\theta)p$. For a many-electron atom, $\boldsymbol{d}(\boldsymbol{p})$ accounts

for electron screening within the atom, depends on the final ionic state, and describes the rearrangement of bound electrons during the release of a single electron. The g_n and h functions are defined as

$$
g_n(t, T, p, \theta) = e^{i\Phi(t - T, t + T, p)} E_z(t - T) E_z(t + T) \int_0^{2\pi} d\phi \cos^n\phi \, d_z^*
$$
$$
\times \left(\boldsymbol{p} + \boldsymbol{e}_z A_z(t - T) \right) d_z \left(\boldsymbol{p} + \boldsymbol{e}_z A_z(t + T) \right) \tag{10}
$$

and

$$
h(t, T, p, \theta) = e^{-i\Phi(t, t - 2T, p)} E_z(t - 2T) \int_0^{2\pi} d\phi \cos\phi \, d_z^*
$$
$$
\times \left(\boldsymbol{p} + \boldsymbol{e}_z A_z(t - 2T) \right) d_x \left(\boldsymbol{p} + \boldsymbol{e}_z A_z(t) \right) \tag{11}
$$

where

$$
\Phi(t_1, t_2, \boldsymbol{p}) = i(t_2 - t_1) I_{\text{p}} + \frac{i}{2} \int_{t_1}^{t_2} dt' \left[\boldsymbol{p} + \boldsymbol{e}_z A_z(t') \right]^2 \tag{12}
$$

and I_{p} is the ionization potential. An equation that is equivalent to our expression for $\Gamma_1(t)$ appears in ref. [14]. Although it is common in theories based on the SFA to reduce the number of integrals using the saddle-point method, we have derived the above expressions without using this approximation, which makes them accurate in a large parameter space. These equations describe single-photon transitions, multiphoton transitions, and quantum tunneling on the same footing. Apart from the SFA, the main assumptions we made in deriving them were to neglect the role of excited bound states and to demand a linear relationship between the probe field and the component of the drift electric current that is parallel to the field.

4. Numerical Experiment

In an ideal NPS measurement, most atoms are ionized by the central half-cycle of the gate pulse, which is possible if the ionization process is highly nonlinear, the gate pulse is not much longer than a single oscillation of its carrier wave, and the central half-cycle of the pulse is significantly stronger than any other half-cycle. For our numerical experiment, we took a gate pulse with a central wavelength of $\lambda_{\text{gate}} = 850$ nm ($\hbar\omega_{\text{gate}} = 1.46$ eV). The pulse intensity had a full width at half maximum (FWHM) of 2.84 fs, and its field had a peak strength of 3.07 V Å^{-1}. Since the purpose of these simulations is to investigate the general properties of NPS (rather than to model a specific experiment), we decided to run them for a hydrogen atom. (To apply our theory to a noble-gas atom, we would have to resort to the single-active-electron approximation, in which case we would have to use a suitable effective atomic potential and numerically evaluate the dipole matrix elements, which are well known for hydrogen.) For the probe pulse, the main constraint is that it must not ionize atoms via single-photon absorption. We chose it to have a central energy of $\hbar\omega_{\text{probe}} = 3.54$ eV, a width of 0.93 fs, and a peak electric
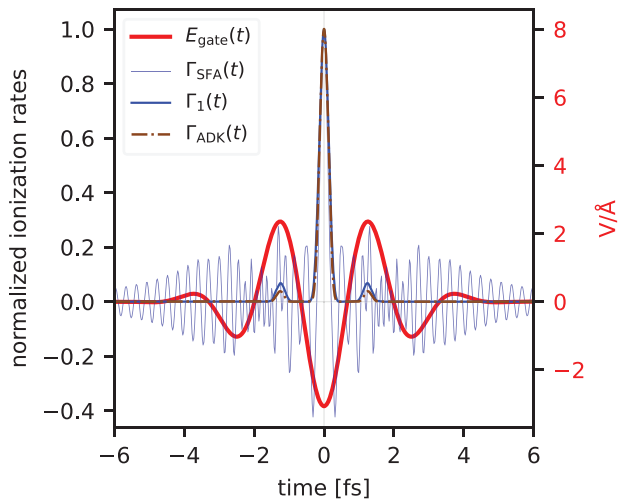
Figure 2. The electric field of the gate pulse (red) and three ionization rates evaluated in the strong-field approximation: Γ_{SFA}, where the fast oscillations allow probe pulses influence the ionization process, $G_1(t)$, which is free from the oscillations, and, for comparison, the quasistatic ADK rate, Γ_{ADK}.

field of 0.008 V Å^{-1}. The vector potentials of both pulses had the same shape

$$A(t) = \frac{E_0}{\omega_0} \cos^8\left(\frac{\pi t}{T}\right) \cos(\omega_0 t - \phi_{\text{CEP}}) \qquad (13)$$

for $\pi|t|/T \leq \pi/2$ and zero outside this interval.

For the numerical solution of the TDSE, we employed the tRecX code.[15] To perform the simulations on a relatively small spatial grid, we used the infinite-range exterior complex scaling method.[16] This method acts as a perfect absorber for an outgoing electron wave packet, while the properties of the wave packet can be determined by recording the values of the time-dependent wave function at the boundary where complex scaling is turned on. We placed this boundary at a distance of 60 atomic units from the ion. The drawback of this method is that it takes a long time for slow electrons to reach the boundary, which makes the calculations prohibitively long. We overcame this problem by using the infinite-time surface flux method.[17] Once the optical fields disappeared, the wave functions inside the unscaled volume were projected onto the exact eigenstates of the atomic potential, allowing the further evolution of the wave packet to be calculated analytically. These calculations gave us $-e \lim_{t\to\infty} \langle \hat{p}(t) \rangle$, which is the contribution of a single atom to the drift current.

5. Results

We derived $\Gamma_{\text{SFA}}(t)$ from the requirement that the quantum-mechanically evaluated $I_{\text{drift}}(\tau)$ must satisfy Equation (2), which we justified using classical mechanics. **Figure 2** shows $\Gamma_{\text{SFA}}(t)$ as described by Equations (6)–(12). The function looks very different from what ionization rates typically look like: it takes both positive and negative values, and it oscillates on the wings of the gate pulse where we do not expect ionization to occur. We explain this behavior in Appendix A as the result of quantum interference

between the wave packets formed by the gate and probe pulses (which requires single-photon ionization by the probe pulse). It should also be noted that, in the quantum treatment, the interaction of the atom with the probe pulse is not decoupled from that with the gate pulse. Even a weak probe field can influence the process of strong-field ionization (for solids, this is known as the Franz–Keldysh effect).

Whether $\Gamma_{\text{SFA}}(t)$ should be called an ionization rate is a semantic question, but its Γ_1 component (thick blue line in Figure 2) has all the attributes of conventional ionization rates: it takes only positive values, it has peaks at the extremes of the gate field, and the magnitudes of these peaks grow rapidly with the peak values of the field's half-cycles. In Appendix B we show that the integral of $\Gamma_1(t)$ is equal to the ionization probability. For comparison, Figure 2 also contains the ionization rate predicted by the Ammosov–Delone–Krainov (ADK) theory[18] (brown curve). The shape of $\Gamma_{\text{ADK}}(t)$ is very similar to that of $\Gamma_1(t)$, and the discrepancy is mainly due to the fact that the ADK rate is a quasistatic one, which is valid only in the tunneling regime, while $\Gamma_1(t)$ is a more general result. For the peak gate field in our simulations, the Keldysh parameter takes a value of 0.9, which is intermediate between the multiphoton and tunneling regimes. While the ADK rate appropriately describes the ionization dynamics in the main half-cycle of the gate pulse, it underestimates the contributions from the weaker neighboring half-cycles. Figure 2 shows us that, for the chosen simulation parameters, the photoionization by the gate pulse is confined to sub-half-cycle time intervals. According to $\Gamma_1(t)$, 89% of the ionization takes place within the central half-cycle of the gate field.

In **Figure 3**, we show the residual average electron velocity in the direction of the probe field, comparing the TDSE and SFA calculations.

We chose to plot the delay dependence of $\langle v_x \rangle$ instead of I_{drift} because the SFA often greatly overestimates the ionization probability. To evaluate the velocities, we divided the electric currents by the respective ionization probabilities and changed the sign of the result because the electron charge is negative. In the SFA, we evaluated the ionization probability by integrating $\Gamma_{\text{SFA}}(t)$ over time. In addition to providing a fair comparison of the TDSE and SFA results, plotting the drift velocities in atomic units allows us to compare them with the vector potential of the probe pulse. We see that, to a first approximation, NPS indeed measures the vector potential, see Equation (1), At the same time, there are notable differences not only in the magnitude of $\langle v_x \rangle(\tau)$ but also in its shape. According to the SFA, $\langle v_x \rangle(\tau)$ is not a replica of $-A_{\text{probe}}(\tau)$, but the two curves reach their three central extrema at practically the same values of τ, and they are both even functions. The TDSE calculations produce a curve that has a somewhat different shape and a smaller amplitude, is shifted toward positive delays, and is not symmetric.
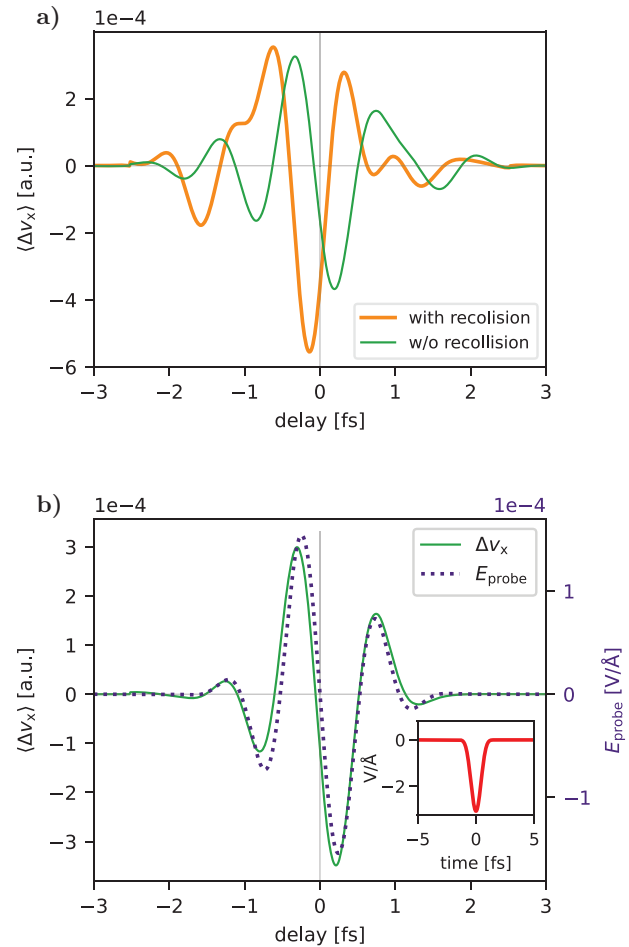
The main reason for the difference between the TDSE and SFA curves in Figure 3a must be the Coulomb interaction between a free electron and its parent ion, which is neglected in the SFA. This interaction is particularly important when the ionizing field changes its sign, decelerates a free electron, and then makes it collide with its parent ion. This process, known as recollision, is responsible for many effects in strong-field physics. In particular, the strong Coulomb attraction at the recollision moment strongly
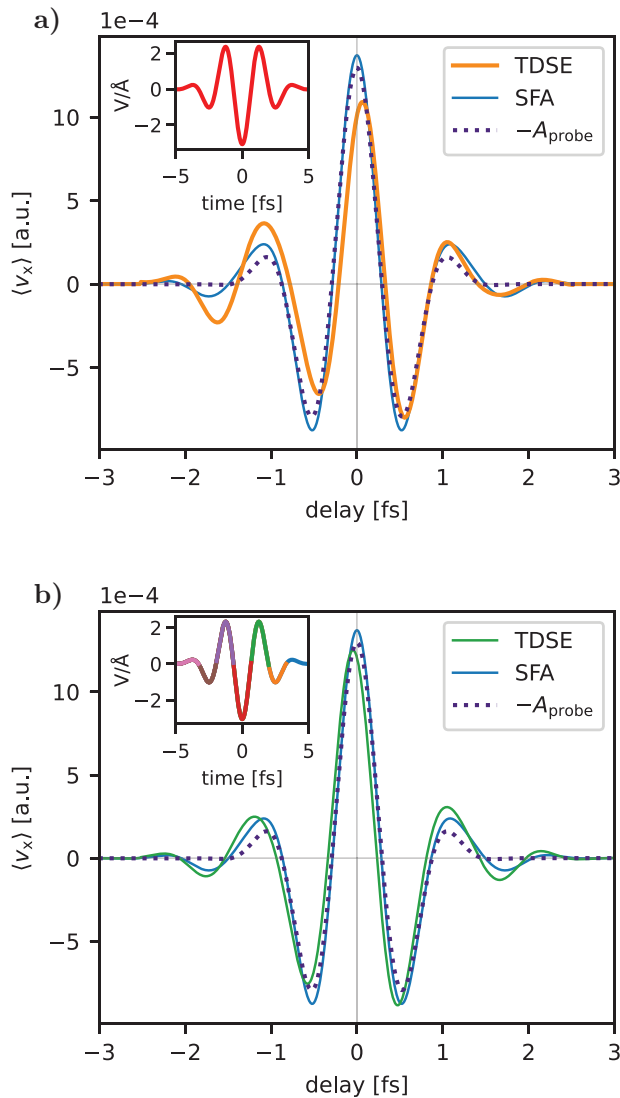
Figure 3. The average velocity of the electron wave packet after the interaction with the light pulses. The plots show how the projection of the drift velocity onto the direction of the probe field depends on the gate-probe delay. a) Simulations with the few-cycle gate pulse (see the inset), where an electron can recollide with its parent ion. b) The sum of $\langle v_x \rangle$ evaluated in simulations with half-cycle gate pulses that, together, produce a pulse that is very similar to the few-cycle gate pulse (see the inset). Here, electrons do not recollide.


Figure 4. The velocity increment acquired by photoelectrons due to the presence of the ionic Coulomb potential. a) A comparison of the simulations with the few-cycle gate pulse, where recollisions occur, with the sum of $\langle \Delta v_x \rangle$ in the simulations with the half-cycle gate pulses, where recollisions do not occur. b) In the simulations with a single half-cycle gate pulse (see inset), $\langle \Delta v_x \rangle(\tau)$ has a shape that is very similar to that of $E_x(t)$.

influences electron motion. To see how much recollision matters for NPS, we decomposed the gate pulse into a series of half-cycle pulses, evaluated $\langle v_x \rangle(\tau)$ for each of these half-cycle gate pulses, and summed the results. Since the electric field of a half-cycle pulse never changes sign, there is no recollision. Figure 3b shows the outcomes of these simulations. The SFA results are practically identical to those in Figure 3a, which means that the different half-cycles of the few-cycle gate pulse ionize independently of each other—there are no visible interference effects. The results obtained by numerically solving the TDSE (green curve) are now closer to the SFA ones, but there are still noticeable differences. This means that recollision is important, but the Coulomb in-

teraction between an electron and an ion shortly after ionization also matters.

The effect of recollision is more evident in **Figure 4**a, where we plot the difference between $\langle v_x \rangle(\tau)$ in the TDSE simulations and that in the SFA. Assuming that the electron-ion interaction is the main effect that is responsible for the difference, $\langle \Delta v_x \rangle(\tau)$ represents the x component of the Coulomb force integrated from the moment an electron becomes free to the end of the probe pulse and averaged over all quantum pathways. This plot shows more clearly that the effect of recollision is of a comparable magnitude to that of the Coulomb attraction immediately after the electron is released, but recollision strongly reshapes $\langle \Delta v_x \rangle(\tau)$.

Let us examine the effect of the Coulomb force in the case of a half-cycle gate pulse. Figure 4b shows that the corresponding increase in the drift velocity has a shape that is very similar to that of $E_x(t)$. This observation supports the argument that we used to justify Equation (4): If ionization is caused by a strong electric field, the electron spends a very short time at a distance from the ion where the ionic Coulomb force is significant, so that the effect

ADVANCED
SCIENCE NEWS

www.advancedsciencenews.com

annalen
der physik

www.ann-phys.org
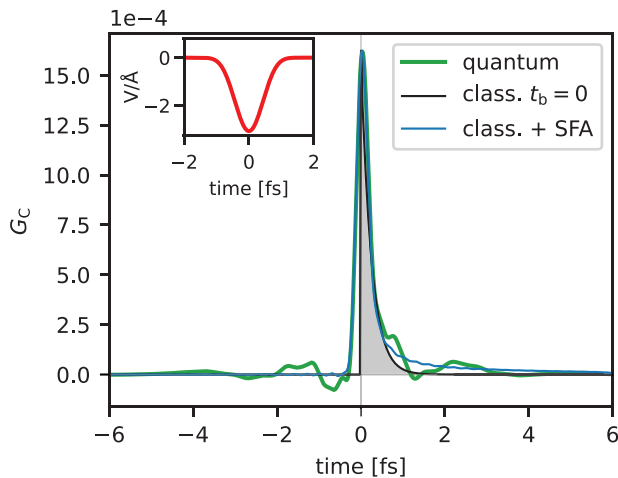
Figure 5. The Coulomb gating function, $G_C(t)$, for a half-cycle gate pulse (see the inset). Here we compare the results obtained by solving the TDSE to the classical ones (see the text for further details).

Figure 6. The magnitude and phase of $G(\omega)$ for the few-cycle gate pulse. The blue curve shows $\Gamma_{SFA}(\omega)$. The green and orange curves represent the numerical solution of the TDSE and the combination of such numerical solutions for a series of half-cycle pulses that, together, approximate the few-cycle gate pulse.

of the force on the x component of the drift velocity is largely determined by the probe field at the moment of ionization.

This insight also largely explains the time shift that we saw in Figure 3b, which looked like there was a delay in photoionization. If both gating functions in Equation (4) are narrow spikes centered at $t = 0$, then $I_{drift}(\tau)$ is a sum of a function that is approximately proportional to $A_x(t)$ and a function that is approximately proportional to $E_x(t)$. For a monochromatic probe field, this would be a weighted sum of $\cos(\omega_{probe}t)$ and $\sin(\omega_{probe}t)$, which is a phase-shifted monochromatic wave. In the terminology used to describe photoemission delays; the time shift in Figure 3b is mostly due to the Coulomb-laser coupling.[19,20]

In addition to the time shift in Figure 3b, there is also a small shift between the two curves in Figure 4b, which occurs because the probe field changes slightly during the time it takes an electron to escape from the vicinity of the ion.

At this point, we can address the question of whether our SFA-based theory correctly predicts ionization dynamics. Without any constraints, the decomposition of G into an ionization rate Γ and a Coulomb gate G_C, summarized in Equation (5), is not unique; one of these components must be known to determine the other. Also, there is no universally applicable way to obtain the ionization rate from a numerical solution of the TDSE, which we could compare to Γ_{SFA}. Nevertheless, we can renormalize Γ_{SFA} by requiring that the ionization probability must be equal to that in the numerical solution of the TDSE, evaluate G_C from Equation (5), and compare the result with the predictions of a classical model for an electron accelerated by the combined field of the light pulses and the ionic Coulomb potential. **Figure 5** visualizes this analysis in the case of a single half-cycle gate pulse (which is free of recollision). The green "quantum" curve in this plot shows $G_C(t)$ obtained by applying deconvolution to the second term on the right-hand side of Equation (4), and we calculated this term by subtracting the drift current evaluated with the properly normalized Γ_{SFA} from the drift current obtained by numerically solving the TDSE. The other two curves show $G_C(t)$ obtained by solving Newton's equations of motion (see Appendix C for details). For
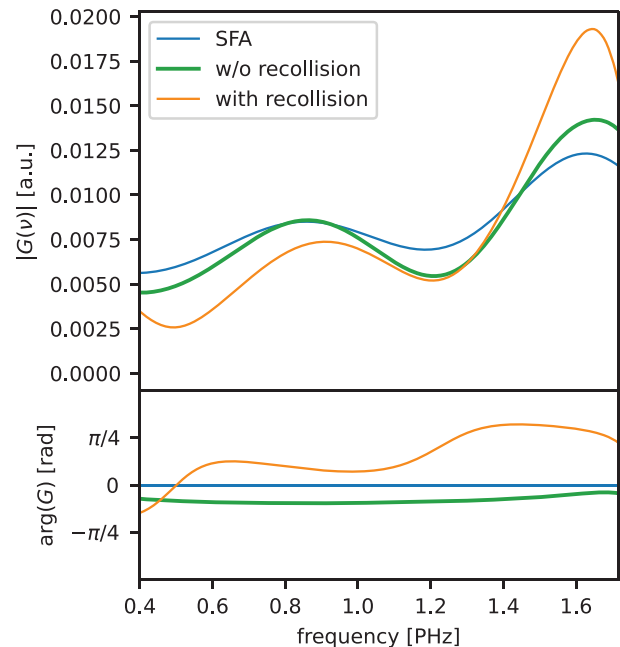
the black "class. $t_b = 0$" curve, we considered a single electron starting its motion at the moment when the gate field is at its peak. For the blue "class. + SFA" curve, we averaged our classical results over birth times using $\Gamma_1(t)$ as the weighting function. The fact that we were able to reproduce the quantum result with the classical analysis provides strong evidence that the renormalized $\Gamma_1(t)$ rate indeed accurately describes the dynamics of ionization, which is consistent with recent work on Coulomb-corrected SFA.[21]

For the few-cycle pulse, the deconvolution that we performed for Figure 5 is problematic. Since our SFA model does not consider excited bound states, we can compare our SFA results with those obtained by numerically solving the TDSE only for probe pulses that do not excite atoms via single-photon transitions. This condition imposes a limit on the highest frequency, for which we can calculate $G_C(\omega)$. There are also technical difficulties that limit the available low frequencies: the spectral intensity of light pulses that can be used for tRecX calculations must be zero at $\omega = 0$. Performing the deconvolution, therefore, requires extrapolation. In the case of the single half-cycle pulse, the good agreement with the classical model allowed us to use the classical analysis for the extrapolation. For the few-cycle pulse, the deconvolution problem is more challenging, especially if recollision is important. For this reason, we present the gating functions in the frequency domain, see **Figure 6**. In the strong-field approximation, the phase of $G(\omega)$ is zero. The Coulomb interaction of an outgoing electron with the ion decreases the phase, while recollision increases it. We also see that the electron-ion interaction decreases the magnitude of the spectral-response function at low frequencies and increases it at high frequencies, especially

if recollisions occur. The decrease in $|G(\omega)|$ at low frequencies is because the Coulomb attraction counteracts the force exerted on an electron by the probe field. The increase in $|G(\omega)|$ at high frequencies means that the Coulomb interaction provides additional gating, which can be confined to even shorter time intervals than that of strong-field ionization.

6. Conclusions

Although the main motivation for this work was to develop a theory for photoconductive sampling, we regard Equations (6)–(12) for the ionization rate as our most general result, which may have other applications, especially in the field of attosecond physics. Apart from the strong-field approximation, we made as few assumptions as possible to derive these equations. In particular, we did not use the saddle-point integration, which makes the ionization rates applicable in various regimes, from single-photon through multiphoton to tunneling. Our numerical simulations provide evidence that these equations accurately describe the ionization dynamics, but they are insufficient for modeling photoconductive sampling because the electron-ion interaction, which the strong-field approximation neglects, is essential for the formation of the drift electric current. We have proposed an ansatz for interpreting photoconductive-sampling measurements: Equations (4) and (5). In our numerical simulations, we were able to separate the effect of electron-ion recollision from the effect of the Coulomb force on an outgoing electron immediately after ionization. For a single ionization event and in the absence of recollision, we showed that a simple classical model can reproduce the role of the Coulomb force in photoconductive sampling. Recollisions increase the complexity of the process, but they also provide an additional gating mechanism that makes NPS more sensitive at frequencies above 1 PHz.

APPENDIX

Appendix A: Photoconductive Sampling in the Strong-Field Approximation

We describe atomic photoionization by solving the time-dependent Schrödinger equation (TDSE) in the dipole approximation:

$$i\frac{\partial}{\partial t}|\Psi\rangle = (\hat{H}_{atom}(t) - \hat{d} \cdot E(t))|\Psi\rangle \tag{A1}$$

which we have written in atomic units using the length gauge; $\hat{H}_{atom}$ is the Hamiltonian describing the unperturbed atom, $E(t)$ is an external electric field (at the position of the atom), and $\hat{d}$ is the electric-dipole operator. Our goal is to find an analytical solution for the electron wave packet formed by ionization, evaluate the x component of its average electron momentum $\langle \hat{p} \rangle$, and then obtain Equations (6)–(12) from the delay dependence of $\langle \hat{p}_x \rangle$. We accomplish this goal by using the strong-field approximation (SFA), where the interaction of a free electron with the external electric field is considered to be much more important than its Coulomb interaction with the ion. If we omit $\hat{H}_{atom}(t)$ in Equation (A1), it has a well-known analytical solution: the Volkov states. At any moment in time, a Volkov state is an eigenstate of the momentum operator, $|p\rangle$. The eigenvalue p and the phase of the state, however, change with time. Using Volkov states to apply the S-matrix method to solve Equation (A1) yields, in first approximation, the following well-known[22] expression for the wave packet produced by

ionization:

$$\lim_{t\to\infty}|\Psi(t)\rangle = -i\int d^3p\,|p\rangle\int_{-\infty}^{\infty}dt'\,e^{-\frac{i}{2}\int_{t'}^{\infty}[p+A(t')]^2\,dt'}e^{iI_p t'}$$
$$\times\langle p + A(t')|d\cdot E(t')|\Psi_0\rangle \tag{A2}$$

where $|\Psi_0\rangle$ is the initial state, which is the atomic ground state in our case, and I_p is the atomic ionization potential. Equation (A2) neglects the depletion of the initial state, that is, it is valid only for small ionization probabilities. The equation also neglects ionization via intermediate transitions to excited bound states (resonance-enhanced multiphoton ionization).

The x component of the drift electron momentum is, by definition, $\langle p_x \rangle = \lim_{t\to\infty}\langle\Psi(t)|\hat{p}_x|\Psi(t)\rangle$. With the aid of Equation (A2) and the normalization condition $\langle p|p'\rangle = \delta(p - p')$, we obtain

$$\langle\hat{p}_x\rangle = \int d^3p'\,(e_x\cdot p')\iint_{-\infty}^{\infty}dt_1\,dt_2\left\{e^{i(t_2-t_1)I_p+\frac{i}{2}\int_{t_1}^{t_2}dt'\,[p'+A(t')]^2}\right.$$
$$\left.\times\left(E(t_1)\cdot d^*(p'+A(t_1))\right)\left(E(t_2)\cdot d(p'+A(t_2))\right)\right\} \tag{A3}$$

where the dipole transition matrix element is defined as $d(p) = \langle p|\hat{d}|\Psi_0\rangle$. From this point on, we consider the gate and probe fields to be polarized along the z- and x-axes, respectively. Let us change the integration variables to $t = (t_2 + t_1)/2$, $T = (t_2 - t_1)/2$, and $p = p' + e_x A_x(t)$. In polar coordinates, we obtain

$$\langle\hat{p}_x\rangle = 2\iint_{-\infty}^{\infty}dt\,dT\int_0^{\infty}dp\,p^2\int_0^{\pi}d\theta\sin\theta\int_0^{2\pi}d\phi$$
$$\times\left\{e^{i\alpha(t,T,p,\theta,\phi)}(p\sin\theta\cos\phi - A_x(t))\right.$$
$$\times\left(E(t-T)\cdot d^*(p+A(t-T)-e_x A_x(t))\right)$$
$$\left.\times\left(E(t+T)\cdot d(p+A(t+T)-e_x A_x(t))\right)\right\} \tag{A4}$$

with

$$\alpha(t,T,p,\theta,\phi) = 2I_p T + \frac{1}{2}\int_{t-T}^{t+T}dt'\left\{p^2 + A_z^2(t') + \left(A_x(t')-A_x(t)\right)^2\right.$$
$$\left.+ 2p\left(A_z(t')\cos\theta + \left(A_x(t')-A_x(t)\right)\sin\theta\cos\phi\right)\right\} \tag{A5}$$

Let us define

$$\Delta(t,t') = A_z(t+t')e_z + [A_x(t+t')-A_x(t)]e_x \tag{A6}$$

$$\bar{\Delta}_x(t,T) = \int_{-T}^{T}dt'\left(A_x(t+t')-A_x(t)\right) \tag{A7}$$

$$\beta(t,T,p) = \exp\left\{i\Phi(t-T,t+T,p) + \frac{i}{2}\int_{t-T}^{t+T}dt'\,\Delta_x^2(t,t')\right\} \tag{A8}$$

where Φ is given by Equation (12). We can rewrite the exponential term in Equation (A4) using the Jacobi–Anger expansion

$$e^{i\alpha(t,T,p,\theta,\phi)} = \beta(t,T,p)\sum_{n=-\infty}^{\infty}i^n J_n\left(p\sin\theta\,\bar{\Delta}_x(t,T)\right)e^{in\phi} \tag{A9}$$

Now we can take the limit of a weak probe pulse by demanding that $\langle\hat{p}_x\rangle$ must depend linearly on $E_x(t)$ and $A_x(t)$. As a first step, we expand the Bessel functions into Taylor series and keep only the terms that are linear

2300322 (7 of 10)

with respect to the probe field:

$$\sum_{n=-\infty}^{\infty} i^n J_n\left(p\sin\theta\,\bar{\Delta}_x(t,T)\right)e^{in\phi}$$

$$= \sum_{n=-\infty}^{\infty}\sum_{m=0}^{\infty} \frac{i^n e^{in\phi}(-1)^m}{m!(n+m+1)!}\left(\frac{p\bar{\Delta}_x\sin\theta}{2}\right)^{2m+n}$$

$$\approx 1 + ip\sin\theta\,\bar{\Delta}_x(t,T)\cos\phi. \tag{A10}$$

Using this approximation for $e^{i\alpha(t,T,p,\theta,\phi)}$ in Equation (A4) and eliminating further terms that are nonlinear with the probe field, we arrive at the following equations:

$$\langle p_x^{(\text{SFA})}\rangle = \langle p_1\rangle + \langle p_2\rangle + \langle p_3\rangle \tag{A11}$$

$$\langle p_1\rangle = -2\int_{-\infty}^{\infty}dt\,A_x(t)\int_0^{\infty}dp\int_0^{\pi}d\theta\,p^2\sin\theta\int_{-\infty}^{\infty}dT\,\beta(t,T,\boldsymbol{p})Z_0(t,T,p,\theta) \tag{A12}$$

$$\langle p_2\rangle = 2i\int_{-\infty}^{\infty}dt\int_0^{\infty}dp\int_0^{\pi}d\theta\,p^4\sin^3\theta\int_{-\infty}^{\infty}dT\,\beta(t,T,\boldsymbol{p})\,\bar{\Delta}_x(t,T)Z_2(t,T,p,\theta) \tag{A13}$$

$$\langle p_3\rangle = 2\int_{-\infty}^{\infty}dt\int_0^{\infty}dp\int_0^{\pi}d\theta\,p^3\sin^2\theta\int_{-\infty}^{\infty}dT\,\beta(t,T,\boldsymbol{p})$$
$$\times\left\{X_1(t,T,p,\theta)+X_1^*(t,-T,p,\theta)\right\} \tag{A14}$$

In these equations, we have introduced the following notation

$$Z_n(t,T,p,\theta) = E_z(t-T)E_z(t+T)$$
$$\times\int_0^{2\pi}d\phi\cos^n\phi\,d_z^*\left(\boldsymbol{p}+\boldsymbol{\Delta}(t,-T)\right)d_z\left(\boldsymbol{p}+\boldsymbol{\Delta}(t,T)\right) \tag{A15}$$

$$X_n(t,T,p,\theta) = E_z(t-T)E_x(t+T)$$
$$\times\int_0^{2\pi}d\phi\cos^n\phi\,d_z^*\left(\boldsymbol{p}+\boldsymbol{\Delta}(t,-T)\right)d_x\left(\boldsymbol{p}+\boldsymbol{\Delta}(t,T)\right) \tag{A16}$$

From these equations, we want to obtain an analytical expression for the ionization rate that satisfies Equation (2), which we write in atomic units as

$$p_x^{(\text{SFA})}(\tau) = -\int_{-\infty}^{\infty}\Gamma(t-\tau)A_x(t)\,dt \tag{A17}$$

To explicitly account for the gate-probe delay τ, we substitute $E_z(t)$ with $E_z(t-\tau)$ and $A_z(t)$ with $A_z(t-\tau)$ in Equations (A6)–(A16). Equation (A12) already has the desired form: it is an integral over time, where the integrand is the product of $A_x(t)$ and a function that depends on τ once the substitutions are performed. For the matrix elements, it is valid to assume that $d_z\left(\boldsymbol{p}+\boldsymbol{\Delta}(t,t')\right) = d_z\left(\boldsymbol{p}+A_z(t-\tau)\boldsymbol{e}_z+(A_x(t+t')-A_x(t))\boldsymbol{e}_x\right)\approx d_z\left(\boldsymbol{p}+A_z(t-\tau)\boldsymbol{e}_z\right)$ if $\max|A_x(t)|\ll\max|A_z(t)|$. These assumptions immediately yield Equation (7).

To derive Equation (8), we additionally need to exchange the integrals over t and t' in Equation (A13) to obtain the desirable form.

The derivation of Equation (9) also involves the change in the order of integrals in Equation (A14), but it requires an additional step: since the probe pulse is represented by its electric field (rather than vector potential) in Equation (A14), we write $E_x(t) = -A_x'(t)$ and integrate by parts to obtain an expression where $A_x(t)$ appears in the integrand of the outermost integral.

Because of the integration over T in Equations (7)–(9), the ionization rate at time t depends on the ionizing field before and after t. However, the integrand is a rapidly oscillating function, and the frequency of its oscillations increases with $|T|$, especially in the limit of tunneling ionization. Therefore, only a small interval of T centered at $T = 0$ makes a significant contribution to Γ_{SFA}.

The plot of $\Gamma_{\text{SFA}}(t)$ in Figure 2 may appear counter-intuitive: the function has long oscillatory tails that extend into the area where the gate field is zero. The frequency of these oscillations is close to the atomic ionization potential. We observe this behavior only in $\langle p_3(\tau)\rangle$ and $\Gamma_3(t)$, and it appears in $\langle p_3(\tau)\rangle$ only if the probe pulse is capable of single-photon ionization. Unlike their counterparts ($\langle p_1(\tau)\rangle$, $\langle p_2(\tau)\rangle$, $\Gamma_1(t)$, and $\Gamma_2(t)$), $\langle p_3(\tau)\rangle$ and $\Gamma_3(t)$ involve not only $d_z(\boldsymbol{p})$ but also $d_x(\boldsymbol{p})$, which is responsible for transitions driven by the probe pulse. These observations suggest that the quantum interference between the wave packets formed by the sole gate and probe pulses is responsible for the oscillations in the drift velocity that do not require the pulses to overlap. Let us illustrate this mechanism by considering the following two Gaussian wave packets evolving without any influence from the ionic potential or an external electric field:

$$\langle\boldsymbol{p}|\Psi_{\text{gate}}(t)\rangle = 2\sqrt{\frac{2a_1^3}{\pi^3}}e^{-a_1p^2}e^{-iI_p\tau}e^{-i\frac{p^2}{2}(t-\tau)}$$

$$\langle\boldsymbol{p}|\Psi_{\text{probe}}(t)\rangle = 2\sqrt{\frac{2a_2^3}{\pi^3}}e^{-a_2(p-e_xp_0)^2}e^{-i\frac{p^2}{2}t} \tag{A18}$$

We assume that the two wave packets are formed by a gate pulse that arrives at time $t = \tau$ and a probe pulse that arrives at $t = 0$, so that the initial state accumulates a phase of $-I_p\tau$ between the pulses. Furthermore, we assume that the wave packet formed by the probe pulse, $\langle\boldsymbol{p}|\Psi_{\text{probe}}(t)\rangle$, propagates along the x axis with an average momentum of p_0. The average momentum for the superposition of the two wave packets does not depend on t, but it depends on τ:

$$\langle p_x(\tau)\rangle = \langle\Psi_{\text{gate}}(t)+\Psi_{\text{probe}}(t)|\hat{p}_x|\Psi_{\text{gate}}(t)+\Psi_{\text{probe}}(t)\rangle$$

$$= p_0 + \frac{16}{\pi^3}(a_1a_2)^{3/2}\int d^3p\,p_x e^{-a_1p^2}e^{-a_2(p-e_xp_0)^2}\cos\left(I_p\tau-\frac{p^2}{2}\tau\right) \tag{A19}$$
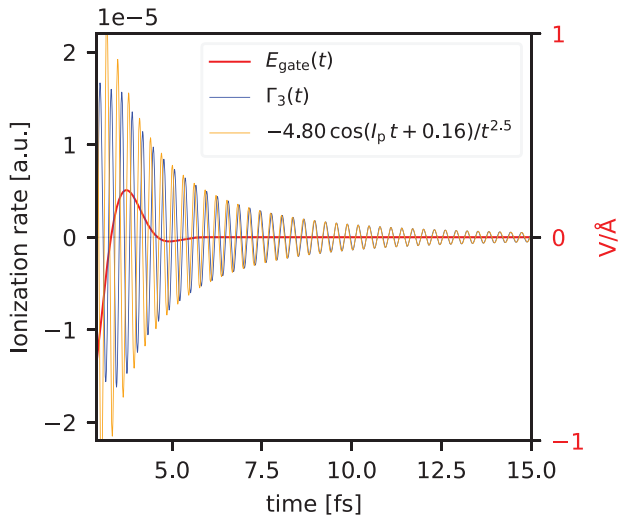
The integral can be taken analytically and, for large values of $|\tau|$, we get the following approximation:

$$\langle p_x(\tau)\rangle \approx p_0\left(1 - 64\sqrt{2}\pi^{-3/2}a_1^{3/2}a_2^{5/2}e^{-a_2p_0^2}\frac{\cos\left(I_p\tau-\frac{\pi}{4}\right)}{\tau^{5/2}}\right) \tag{A20}$$

We see that even though the field of the gate pulse exerts no force along the x-axis, the electron wave packet created by the pulse can interfere with that created by the probe pulse making the residual current depend on the gate-probe delay.

The interference results in oscillations with a frequency of I_p. As the delay increases, the amplitude of these oscillations decreases according to $\tau^{-5/2}$.

**ADVANCED
SCIENCE NEWS**

www.advancedsciencenews.com

annalen
der **physik**

www.ann-phys.org

Figure A1. The approximation of $\Gamma_3(t)$ at the end of the gate pulse by $\cos(I_p t + \varphi)/t^{5/2}$, which describes the interference of wave packets independently formed by the gate and probe pulses.

Although the probe field does not explicitly enter the expression for $\Gamma_3(t)$, this part of the gating function describes this kind of interference because

$$p_3(\tau) = -\int_{-\infty}^{\infty} \Gamma_3(t-\tau) A_x(t_b)\, dt \qquad (A21)$$

for an arbitrary probe pulse. In **Figure** A1 we show that $\Gamma_3(t)$ indeed has the $\cos(I_p t + \varphi)/t^{5/2}$ asymptotic behavior.

Appendix B: The Ionization Probability in our SFA Model

Here we sketch the proof that the integral of $\Gamma_1(t)$, defined by Equation (7), is the ionization probability by the gate pulse within the SFA if the ground-state depletion is negligible. Let us repeat the same derivation as in Appendix A, but without the probe pulse ($A = A_z e_z$) and with the unity operator, $\hat{1}$, in the place of $\hat{p}_x$. This derivation must produce the ionization probability in the form of an integral over time:

$$\lim_{t\to\infty}\langle\Psi(t)|\hat{1}|\Psi(t)\rangle = \int_{-\infty}^{\infty}\Gamma_{\text{gate}}(t)\,dt = \int d^3p' \iint_{-\infty}^{\infty} dt_1\, dt_2$$

$$\times\left\{ e^{i(t_2-t_1)I_p + \frac{i}{2}\int_{t_1}^{t_2} dt'\,[p'+e_z A_z(t')]^2} \right.$$

$$\times\, E_z(t_1) d_z^*\left(p' + e_z A_z(t_1)\right) E_z(t_2) d_z\left(p' + e_z A_z(t_2)\right)\Big)\Big\}$$

$$= 2\int_{-\infty}^{\infty} dt \int_{-\infty}^{\infty} dT \int_0^{\infty} dp\, p^2 \int_0^{\pi} d\theta \sin\theta \int_0^{2\pi} d\phi$$

$$\times\left\{ e^{i\Phi(t-T,t+T,p)} E_z(t-T) d_z^*\left(p + e_z A_z(t-T)\right) \right.$$

$$\times\, E_z(t+T) d_z\left(p + e_z A_z(t+T)\right)\Big\} \qquad (B1)$$

Obviously,

$$\Gamma_{\text{gate}}(t) = 2\int_0^{\infty} dp\, p^2 \int_0^{\pi} d\theta \sin\theta \int_{-\infty}^{\infty} dT$$

$$\times\left\{ e^{i\Phi(t-T,t+T,p)} E_z(t-T) E_z(t+T) \right.$$

$$\times\int_0^{2\pi} d\phi\, d_z^*\left(p + e_z A_z(t-T)\right) d_z\left(p + e_z A_z(t+T)\right)\Big\} \qquad (B2)$$

which is equivalent to Equation (7).

If Γ_1 is the rate that, once integrated, yields the ionization probability, what are then the roles of Γ_2 and Γ_3? If $\lim_{t\to\pm\infty} A_z(t) = 0$, it is obvious that

$$\int_{-\infty}^{\infty} \Gamma_3(t)\, dt = 0 \qquad (B3)$$

In our numerical simulations, we also see that the integral of $\Gamma_2(t)$ is orders of magnitude smaller than that of $\Gamma_1(t)$. Since these two terms play no detectable role in the absence of the probe pulse, they must be responsible for effects that emerge when both pulses are present, even though none of the three rates explicitly depends on the probe pulse.

Appendix C: Classical Coulomb-Laser Correction

Let us consider the motion of a classical electron in the combined electric field of the light pulses, $E(t)$, and the field of the singly-charged ion placed at $r = 0$. In atomic units, which we use throughout this section, the force acting on an electron at position r is equal to

$$F(r) = -\frac{r}{|r|^3} - E \qquad (C1)$$

Solving Newton's equation of motion, $\ddot{r} = F(r(t))$, we can calculate the velocity that a classical electron acquires in the limit $t \to +\infty$. Subtracting from this value the velocity that an electron would acquire in the absence of the interaction with the ion, we obtain the classical correction due to Coulomb-laser coupling, Δv^{class}, which depends on the gate-probe delay τ. For a weak probe pulse, we expect a linear relationship between $\Delta v^{\text{class}}(\tau)$ and $E_x(t)$. Indeed, if $|x| \ll |z|$ and $\gamma = 0$, then the x component of the Coulomb force equals

$$-\frac{x}{|r|^3} \approx -\frac{x}{|z|^3} \qquad (C2)$$

Thus, for the electron velocity along the probe field, the approximation

$$v_x'(t) \approx -\frac{x(t)}{|z(t)|^3} - E_x(t) \qquad (C3)$$

is valid at least until a recollision occurs. A recollision may strongly deflect an electron, but, for most trajectories, the electron then quickly leaves the region of a strong Coulomb attraction, so we obtain

$$\Delta v_x^{\text{class}} \approx -\int_{t_0}^{\infty} dt\, \frac{x(t)}{|z(t)|^3} \qquad (C4)$$

As long as the probe pulse is too weak to have a significant effect on $z(t)$ (until a recollision occurs), Δv^{class} is linear with respect to $x(t)$, which is linear with respect to $E_x(t)$. Even though the Coulomb force decreases with an increasing electron-ion distance, $|F_x|$ increases with $|x|$, and larger values of the electron displacement along the x-axis cause larger values of $\Delta v_x^{\text{class}}$.

To prepare Figure 5, we solved Newton's equations numerically without assuming small $|x|$. We found that a good agreement with the TDSE simulations was possible only if we allowed the probe field to influence the initial position of the electron trajectory, $r(t_0)$ (otherwise, the x component of the Coulomb force is zero at t_0, which underestimates the effect of the Coulomb force on the electron's motion along the x-axis). We chose $r(t_0)$ to be the point where the classically forbidden region ends along the line

**ADVANCED
SCIENCE NEWS**

www.advancedsciencenews.com

*annalen
der* **physik**

www.ann-phys.org

that passes through $r = 0$ in the direction of $E(t_0)$, which is the combined field of both pulses at the birth moment. Here is the expression for this initial condition:

$$r(t_0) = -\frac{E(t_0)}{|E(t_0)|} \frac{|I_p| + \sqrt{I_p^2 - 4|E(t_0)|}}{2|E(t_0)|} \tag{C5}$$

To keep our classical model as simple as possible, we did not average over an ensemble to electron trajectories with different initial conditions. Instead, we adjusted the initial velocity, which we took to be along the y-axis. The results shown in Figure 5 were obtained with $v(t_0) = 0.5e_y$.

Acknowledgements

Conflict of Interest

The authors declare no conflict of interest.

Data Availability Statement

The data that support the findings of this study are available from the corresponding author upon reasonable request.

Keywords

[1] E. Goulielmakis, M. Uiberacker, R. Kienberger, A. Baltuska, V. Yakovlev, A. Scrinzi, T. Westerwalbesloh, U. Kleineberg, U. Heinzmann, M. Drescher, F. Krausz, *Science* **2004**, *305*, 1267.

[2] K. T. Kim, C. Zhang, A. D. Shiner, B. E. Schmidt, F. Légaré, D. M. Villeneuve, P. B. Corkum, *Nat. Photonics* **2013**, *7*, 958.

[3] A. S. Wyatt, T. Witting, A. Schiavi, D. Fabris, P. Matia-Hernando, I. A. Walmsley, J. P. Marangos, J. W. G. Tisch, *Optica* **2016**, *3*, 303.

[4] S. Keiber, S. Sederberg, A. Schwarz, M. Trubetskov, V. Pervak, F. Krausz, N. Karpowicz, *Nat. Photonics* **2016**, *10*, 159.

[5] P. Carpeggiani, M. Reduzzi, A. Comby, H. Ahmadi, S. Kühn, F. Calegari, M. Nisoli, F. Frassetto, L. Poletto, D. Hoff, J. Ullrich, C. D. Schröter, R. Moshammer, G. G. Paulus, G. Sansone, *Nat. Photonics* **2017**, *11*, 383.

[6] S. B. Park, K. Kim, W. Cho, S. I. Hwang, I. Ivanov, C. H. Nam, K. T. Kim, *Optica* **2018**, *5*, 402.

[7] S. Sederberg, D. Zimin, S. Keiber, F. Siegrist, M. S. Wismer, V. S. Yakovlev, I. Floss, C. Lemell, J. Burgdörfer, M. Schultze, F. Krausz, N. Karpowicz, *Nat. Commun.* **2020**, *11*, 430.

[8] D. Zimin, M. Weidman, J. Schötz, M. F. Kling, V. S. Yakovlev, F. Krausz, N. Karpowicz, *Optica* **2021**, *8*, 586.

[9] D. A. Zimin, V. S. Yakovlev, N. Karpowicz, *Sci. Adv.* **2022**, *8*, eade1029.

[10] K. Arai, D. Okazaki, I. Morichika, S. Ashihara, *ACS Photonics* **2023**, *10*, 1702.

[11] A. Schiffrin, T. Paasch-Colberg, N. Karpowicz, V. Apalkov, D. Gerster, S. Mühlbrandt, M. Korbman, J. Reichert, M. Schultze, S. Holzner, J. V. Barth, R. Kienberger, R. Ernstorfer, V. S. Yakovlev, M. I. Stockman, F. Krausz, *Nature* **2013**, *493*, 70.

[12] J. Schötz, A. Maliakkal, J. Blöchl, D. Zimin, Z. Wang, P. Rosenberger, M. Alharbi, A. M. Azzeer, M. Weidman, V. S. Yakovlev, B. Bergues, M. F. Kling, *Nat. Commun.* **2022**, *13*, 962.

[13] K. Amini, J. Biegert, F. Calegari, A. Chacón, M. F. Ciappina, A. Dauphin, D. K. Efimov, C. F. de Morisson Faria, K. Giergiel, P. Gniewek, A. S. Landsman, M. Lesiuk, M. Mandrysz, A. S. Maxwell, R. Moszyński, L. Ortmann, J. A. Pérez-Hernández, A. Picón, E. Pisanty, J. Prauzner-Bechcicki, K. Sacha, N. Suárez, A. Zaïr, J. Zakrzewski, M. Lewenstein, *Rep. Prog. Phys.* **2019**, *82*, 116001.

[14] M. Lewenstein, P. Balcou, M. Y. Ivanov, A. L'huillier, P. B. Corkum, *Phys. Rev. A* **1994**, *49*, 2117.

[15] A. Scrinzi, *Comput. Phys. Commun.* **2022**, *270*, 108146.

[16] A. Scrinzi, *Phys. Rev. A* **2010**, *81*, 053845.

[17] F. Morales, T. Bredtmann, S. Patchkovskii, *J. Phys. B At. Mol. Opt. Phys.* **2016**, *49*, 245001.

[18] M. V. Ammosov, N. B. Delone, V. P. Krainov, in *High Intensity Laser Processes*, Vol. *664*, SPIE, Bellingham, WA **1986**, pp. 138–141.

[19] S. Nagele, R. Pazourek, J. Feist, K. Doblhoff-Dier, C. Lemell, K. Tőkési, J. Burgdörfer, *J. Phys. B At. Mol. Opt. Phys.* **2011**, *44*, 081001.

[20] D. Azoury, M. Krüger, B. D. Bruner, O. Smirnova, N. Dudovich, *Sci. Rep.* **2021**, *11*, 495.

[21] V. Petrović, H. Delibašić Marković, I. Petrović, *Results Phys.* **2023**, *51*, 106718.

[22] M. Y. Ivanov, M. Spanner, O. Smirnova, *J. Mod. Opt.* **2005**, *52*, 165.